

REPORT DOCUMENTATION PAGE			Form Approved OMB No. 0704-0188	
<p>Public reporting burden for this collection of information is estimated to average 1 hour per response, including the time for reviewing instructions, searching existing data sources, gathering and maintaining the data needed, and completing and reviewing this collection of information. Send comments regarding this burden estimate or any other aspect of this collection of information, including suggestions for reducing this burden to Department of Defense, Washington Headquarters Services, Directorate for Information Operations and Reports (0704-0188), 1215 Jefferson Davis Highway, Suite 1204, Arlington, VA 22202-4302. Respondents should be aware that notwithstanding any other provision of law, no person shall be subject to any penalty for failing to comply with a collection of information if it does not display a currently valid OMB control number. PLEASE DO NOT RETURN YOUR FORM TO THE ABOVE ADDRESS.</p>				
1. REPORT DATE (DD-MM-YYYY) May 2012		2. REPORT TYPE Journal Article		3. DATES COVERED (From - To)
4. TITLE AND SUBTITLE Superoleophobic Surfaces through Control of Sprayed - on Stochastic Topography (Pre-Print)		5a. CONTRACT NUMBER In-House		
		5b. GRANT NUMBER		
		5c. PROGRAM ELEMENT NUMBER		
6. AUTHOR(S) Raymond Campos, Andrew J. Guenther, Adam J. Meuler, Anish Tuteja, Robert E. Cohen, Gareth H. McKinley Timothy S. Haddad, and Joseph M. Mabry		5d. PROJECT NUMBER		
		5e. TASK NUMBER		
		5f. WORK UNIT NUMBER Q0AD		
7. PERFORMING ORGANIZATION NAME(S) AND ADDRESS(ES) Air Force Research Laboratory (AFMC) AFRL/RQRP 10 E. Saturn Blvd. Edwards AFB CA 93524-7401		8. PERFORMING ORGANIZATION REPORT NO.		
9. SPONSORING / MONITORING AGENCY NAME(S) AND ADDRESS(ES) Air Force Research Laboratory (AFMC) AFRL/RQR 5 Pollux Drive Edwards AFB CA 93524-7048		10. SPONSOR/MONITOR'S ACRONYM(S)		
		11. SPONSOR/MONITOR'S REPORT NUMBER(S) AFRL-RZ-ED-JA-2012-134		
12. DISTRIBUTION / AVAILABILITY STATEMENT Approved for public release, distribution unlimited.				
13. SUPPLEMENTARY NOTES PA Clearance #: 12304; Cleared 3 May 2012. Langmuir, 2012, 28 (25), pp 9834-9841				
14. ABSTRACT The liquid repellency and surface topography characteristics of coatings comprising a sprayed-on mixture of fluoroalkyl-functional precipitated silica and a fluoropolymer binder were examined using contact and sliding angle analysis, electron microscopy, and image analysis for determination of fractal dimensionality. The coatings proved to be an especially useful class of liquid repellent materials due to their combination of simple and scalable deposition process, low surface energy, and the roughness characteristics of the aggregates. These characteristics interact in a unique way to prevent the buildup of binder in interstitial regions, preserving re-entrant curvature across multiple length scales, thereby enabling a wide range of liquid repellency, including superoleophobicity. In addition, rather than accumulating in the interstices, the binder becomes widely distributed across the surface of the aggregates, enabling a mechanism in which a simple shortage or excess of binder controls the extent of coating roughness at very small length scales, thereby controlling the extent of liquid repellence.				
15. SUBJECT TERMS Superoleophobic Surfaces, Stochastic Topography, Spray				
16. SECURITY CLASSIFICATION OF:			17. LIMITATION OF ABSTRACT SAR	18. NUMBER OF PAGES 35
a. REPORT Unclassified	b. ABSTRACT Unclassified	c. THIS PAGE Unclassified		
				19a. NAME OF RESPONSIBLE PERSON Joseph M. Mabry
				19b. TELEPHONE NO (include area code) N/A

Superoleophobic Surfaces through Control of Sprayed-on Stochastic Topography

Raymond Campos¹, Andrew J. Guenther,^{2} Adam J. Meuler,³ Anish Tuteja,⁴ Robert E. Cohen,⁵ Gareth H. McKinley,⁶ Timothy S. Haddad,¹ and Joseph M. Mabry^{2*}*

¹ERC Incorporated, Air Force Research Laboratory
Edwards AFB, CA 93524

²Propulsion Directorate, Air Force Research Laboratory
Edwards AFB, CA 93524

³National Research Council / Air Force Research Laboratory
Edwards AFB, CA 93524

⁴Department of Materials Science and Engineering, The University of Michigan
Ann Arbor, MI 48109

⁵Department of Chemical Engineering, Massachusetts Institute of Technology
Cambridge, MA 02139

⁶Department of Mechanical Engineering, Massachusetts Institute of Technology
Cambridge, MA 02139

AUTHOR EMAIL ADDRESS andrew.guenther@edwards.af.mil

RECEIVED DATE (to be automatically inserted after your manuscript is accepted if required according to the journal that you are submitting your paper to)

Abstract

The liquid repellence and surface topography characteristics of coatings comprising a sprayed-on mixture of fluoroalkyl-functional precipitated silica and a fluoropolymer binder were examined using contact and sliding angle analysis, electron microscopy, and image analysis for determination of fractal dimensionality. The coatings proved to be an especially useful class of liquid repellent materials due to their combination of simple and scalable deposition process, low surface energy, and the roughness characteristics of the aggregates. These characteristics interact in a unique way to prevent the build-up

of binder in interstitial regions, preserving re-entrant curvature across multiple length scales, thereby enabling a wide range of liquid repellency, including superoleophobicity. In addition, rather than accumulating in the interstices, the binder becomes widely distributed across the surface of the aggregates, enabling a mechanism in which a simple shortage or excess of binder controls the extent of coating roughness at very small length scales, thereby controlling the extent of liquid repellence

1. Introduction

A significant advance in the field of liquid repellence, the creation of surfaces exhibiting superoleophobicity has generated much interest since 2007.¹ The unusual characteristics of superoleophobic surfaces in contact with fuels, oils, and greases, including contact angles in excess of 150°, droplet sliding angles approaching zero, and robust metastability of the partially wetted (Cassie-Baxter) state,²⁻⁵ provide exceptional liquid repellence with applications in machinery,⁶ fabrics,^{7,8} energy efficiency,⁹ and protection from fouling and hazardous materials.¹⁰ After only very sporadic previous reports,¹² researchers have recently created many types of superoleophobic surfaces, with new reports appearing at a very rapid pace.^{1-4,7,8,11,13-27} Fabrication methods involve dip coating, electrospinning,^{1,2,7,8} spray coating,¹⁴ and templating. Among these, spray coating provides the advantages of great simplicity, scalability, speed, and compatibility with almost any substrate type (if post-processing is limited to drying at low temperature and appropriate solvents are selected). Thus, there remains a significant need for further development of superoleophobic surfaces formed by spray coating, as well as for simple means of tuning the liquid repellence of such surfaces.

Herein, we describe the development of a set of materials and methods for producing spray-coated surfaces with liquid repellence characteristics ranging from hydrophobic to superoleophobic (toward hydrocarbons as light as dodecane) that address the challenges of scalable, affordable fabrication and straightforward tuneability. The simple and robust process for fabricating these surfaces utilizes fluoroalkylsilane-treated precipitated silica aggregates (“FF-silica”), the synthesis of which we have previously reported.²⁸ The coating formulation also includes a Viton® fluoropolymer binder, and

a fluorinated solvent (AK-225G). This combination resulted in a wide range of stochastic surface topographies and very low surface energy values. (This combination of materials has also been widely utilized to achieve high levels of abrasion, wear, and scratch resistance.²⁹) Roughness on multiple length scales below 10 μm , along with the propensity to form surfaces with re-entrant curvature, were observed to be key factors that enabled these surfaces to exhibit a wide range of liquid repellency. In addition, the ability to control the fine-scale texture by altering the amount of binder in the system was found to be a convenient geometric tuning mechanism for shaping the liquid repellence characteristics of these randomly textured, sprayed-on surfaces.

2. Materials and Methods

2.1 Preparation of Fluoroalkyl-Functional Silica (FF-Silica): Precipitated silica aggregates (HiSil 233, from PPG Industries) were treated with (1,1,2,2-tetrahydroperfluorodecyl)-dimethylchlorosilane using a previously described method.²⁸ Relevant physical properties of the modified silica aggregates can be found in Table S1 of Supporting Information.

2.2 Spray-Deposition: Coatings were formulated from a stock mixture of 5 mg/mL [®]Viton ETP-600S fluoropolymer (DuPont) in Asahiklin AK-225G (1,3-dichloro-1,2,2,3,3-pentafluoropropane; AGC Chemicals Americas). FF-silica was suspended into this mixture at 0-90 wt% silica/total solids. Additional solvent was added to maintain a total solids concentration of 5 mg/mL. Samples were prepared by spraying thoroughly mixed coating formulations immediately onto 1" silicon wafers (P-type; 100-orientation, Wafer World) through an airbrush (Paasche, VLSTPRO) with a 1.06 mm diameter tip using compressed air (25 psi). The airbrush was repeatedly passed over the substrate laterally at an approximate distance of 15-20 cm from the substrate until 20 mL of the coating mixture had been deposited. The resultant deposition level is around is 20 mg/cm². Following spray coating, samples were air dried for 1 hr followed by drying for 12 hrs at 60 °C (ambient atmosphere) in a laboratory oven.

2.3 Contact Angle Measurements: Advancing (θ_{adv}) and receding (θ_{rec}) contact angles were measured using a VCA 2000 goniometer (AST, Inc.) as probe fluid was added or removed from $\sim 5 \mu\text{L}$ sessile

droplets. Sliding angles were measured with a Rame-Hart Model 590 goniometer on ~15-20 μL droplets. Measurements were made at multiple locations in each sample, with the standard deviation from all measurements being reported as the characteristic uncertainty in Table S2 of Supporting Information. For comparison, additional measurements on several samples with different surface composition/probing liquid combinations were made on a Dataphysics OCA20 goniometer equipped with a TBU90 tilting stage, and no significant differences were found.

2.4 Surface Characterization: Cross-sectioned samples were prepared by embedding coatings in epoxy and then sectioning the embedded sample using a PT-X ultramicrotome (RMC Products) using Boeckeler, Inc. methodology. Gold-sputtered cross-section and plan view (top down) samples were imaged using an FEI Quanta 600 scanning electron microscope.

3. Results and Discussion

The wide range of liquid repellency of the sprayed-on surfaces based on the combination of precipitated silica aggregates, fluoropolymer binder, and AK225G is illustrated in Fig. 1. At low FF-silica loading levels, the Wenzel (fully wetted) state exists for all liquids studied, with advancing contact angles that are typical of highly fluorinated surfaces.^{30,31} As the FF-silica loading level increases, however, the Cassie-Baxter state becomes prevalent, starting at approx. 20 wt% FF-silica for water and, at higher loading levels, for liquids of progressively lower surface tension. As indicated by the more detailed liquid repellence map in Fig. 2, a generally simple, monotonic, and gradual relationship exists between the surface tension of the contacting liquid and the FF-silica loading level required for attaining the Cassie-Baxter state. Although Fig. 2 applies directly only for the specific set of spraying parameters reported herein, it should be noted that the spray process includes an annealing step above the glass transition of the polymer binder, which allows for relaxation of any residual stresses and some equilibration, even after the solvent has evaporated. As a result, we expect that the behavior illustrated in Fig. 2 would exhibit a low sensitivity to variations in processing parameters, provided that a similar overall density of solids is deposited on the surface. The existence of this simple and robust relationship

enables quantification of the trade-offs (often driven by the need to simultaneously satisfy multiple performance criteria) required to obtain a desired degree of liquid repellence, and suggests that even complex, randomly textured surfaces may be systematically altered in a straightforward manner by altering the ratio of aggregates to binder in order to control liquid repellence.

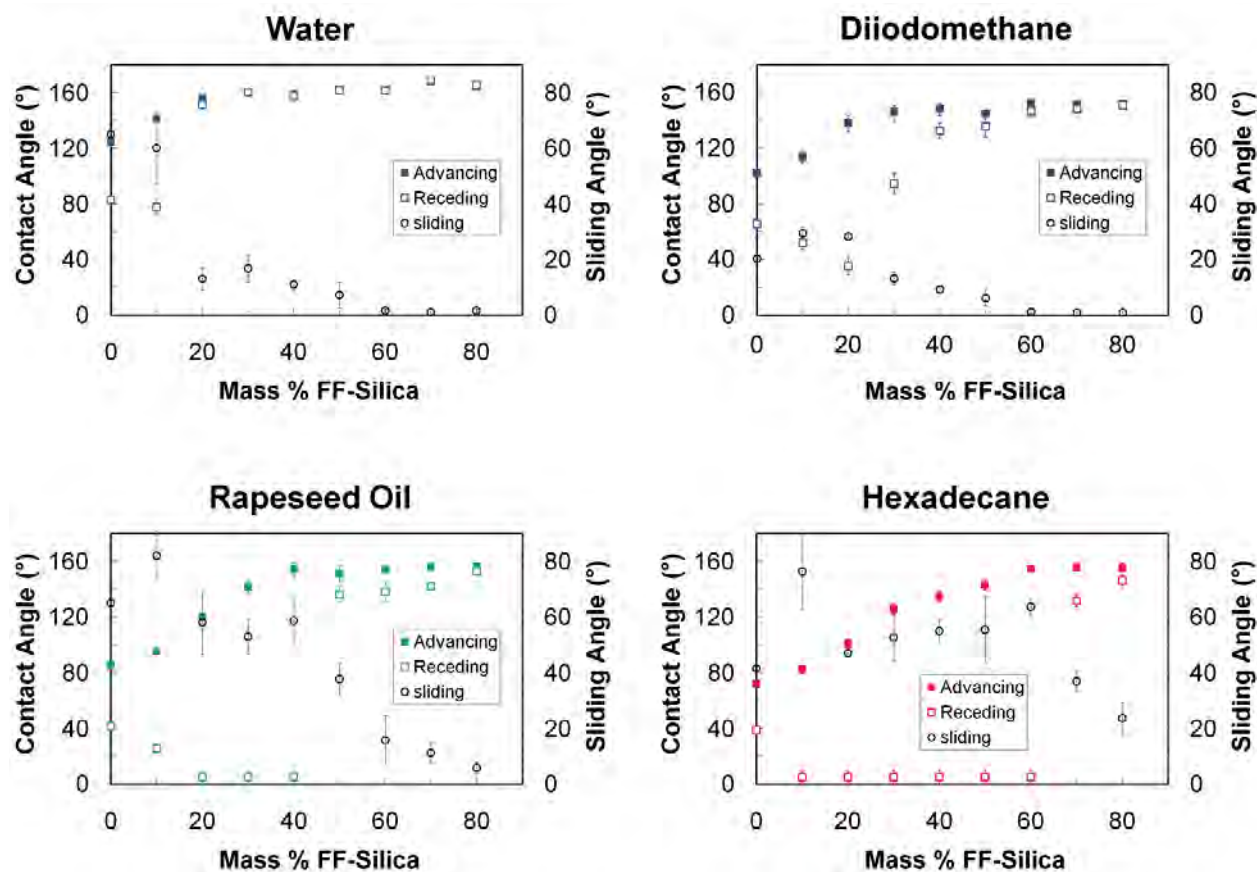


Figure 1. Apparent advancing, receding, and sliding contact angle measurements of water ($\gamma_{lv} = 72.1$ mN/m), diiodomethane ($\gamma_{lv} = 50.8$ mN/m), rapeseed oil ($\gamma_{lv} = 35.5$ mN/m), and hexadecane ($\gamma_{lv} = 27.5$ mN/m) on flat silicon wafers sprayed with mixtures of fluoropolymer and FF-silica.

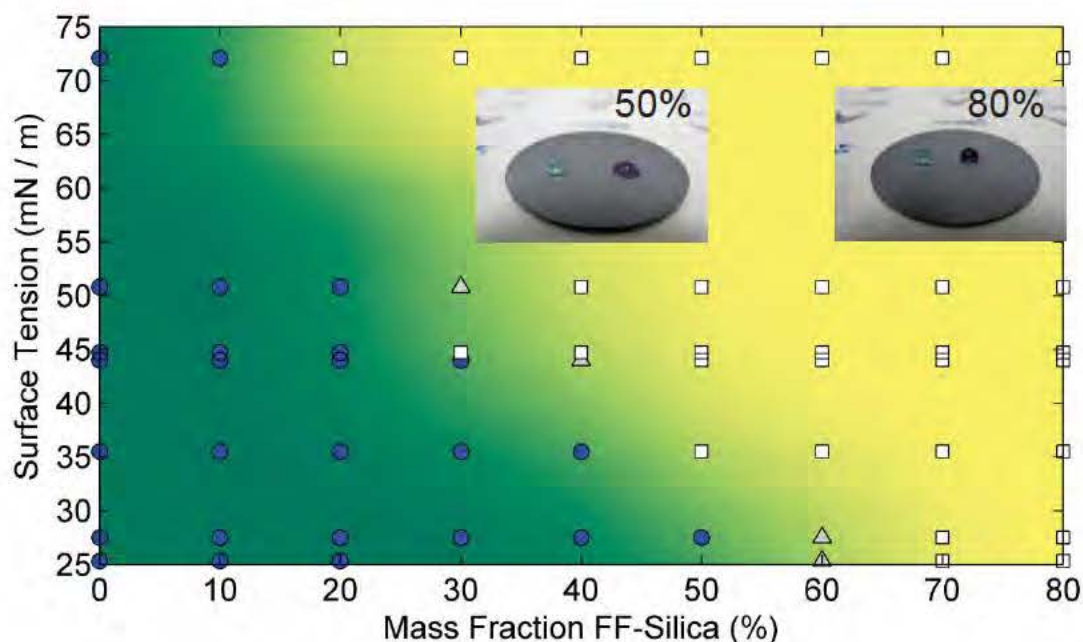


Figure 2. Map depicting the state of liquid contact with FF-silica surfaces as a function of FF-silica loading and surface tension of the contacting liquid; filled circles represent Wenzel states, shaded triangles represent Cassie states with contact angle hysteresis $> 20^\circ$, unfilled squares represent Cassie states with contact angle hysteresis $\leq 20^\circ$. The background color is intended only as an aid for visualization. Inset shows droplets of water (blue) and dodecane (purple) on spray-coated surfaces comprised of 50 wt% FF- silica (left image) and 80 wt% FF-silica (right image) demonstrating the different wetting states as a function of silica loading.

In order to better understand the basis for the simple relationship seen in Fig. 2, the geometry of the sprayed-on surfaces was examined in more detail. Fig. 3 provides both surface view and cross-sectional SEM images of the surfaces as a function of FF-silica loading, with detailed views provided in Fig. 4. An analysis of the fractal dimensionality of the surfaces as determined by the method of Shibuichi¹² is shown in Fig. 5. The images in Figs. 3 and 4 demonstrate that the FF-silica aggregates

(which feature a fluoroalkylated surface to ensure liquid repellence and maintain good dispersion in the spraying solvent) retain sufficient integrity to produce large protrusions from the fluoropolymer layer after deposition and film formation. It also appears that the low surface tension of the carrier solvent, perhaps in combination with the porosity afforded by the aggregates,³² allows the fluoropolymer coating to become conformal, particularly as the FF-silica loading level is increased beyond approx. 40%. In Fig. 4, regions of conformality are indicated by filled arrows, while regions that lack conformality are indicated by unfilled arrows. Since the conformality extends to the base of the protrusions, it appears the typical phenomenon of binder accumulation in the interstitial junctions does not take place. Rather, the protrusions exhibit re-entrant curvature, a key geometric characteristic that enables the Cassie state to be observed with low surface-tension liquids.¹ In addition, the conformality transfers the multi-scale roughness inherent in the aggregates to the coating as a whole. Therefore, the use of silica aggregates in a fluoropolymer binder with a fluorocarbon carrier solvent allows the key characteristic of re-entrant curvature to appear at multiple length scales in sprayed-on FF-silica coatings. In combination with the very low surface energy imparted by the FF-silica and the fluoropolymer, the re-entrant curvature leads to outstanding liquid repellency, including superoleophobicity.

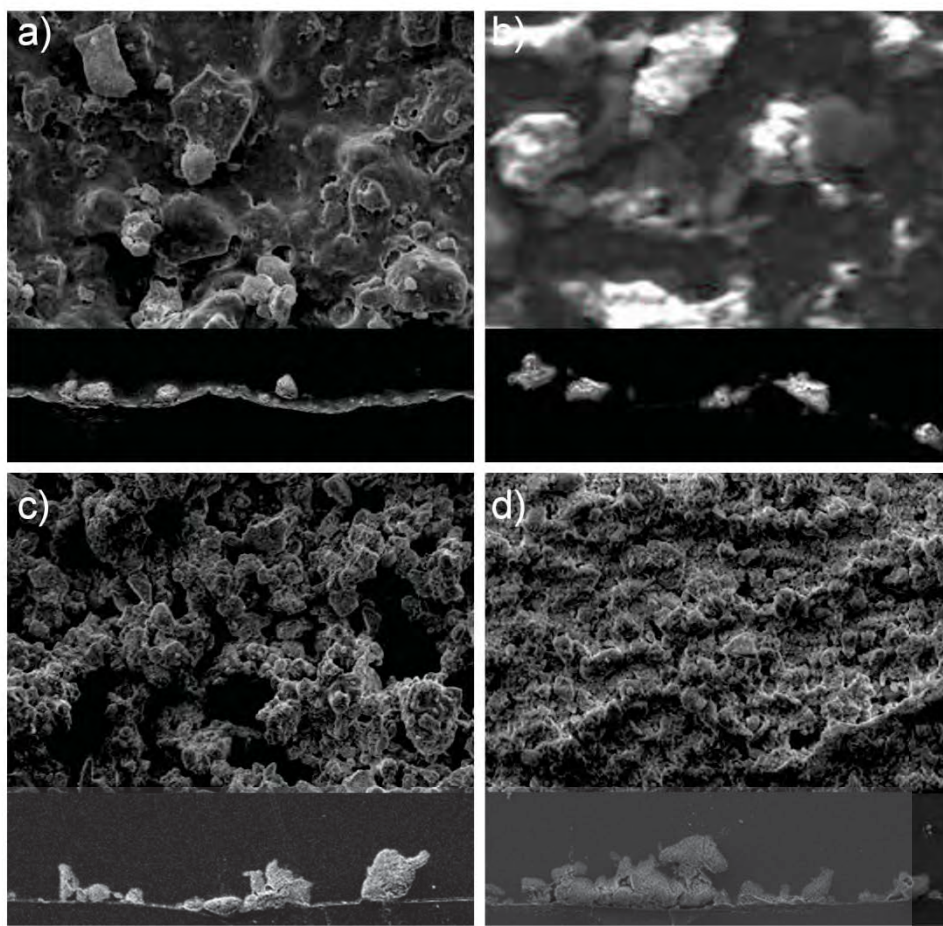


Figure 3. Plan view (top panels) and corresponding cross-sections (lower panels) for FF-silica / fluoroelastomer composites at FF-silica loadings of a) 20 wt% b) 40 wt% c) 60 wt% d) 80 wt%. Note that the images are all at identical magnification, so that the scale bar applies to all images.

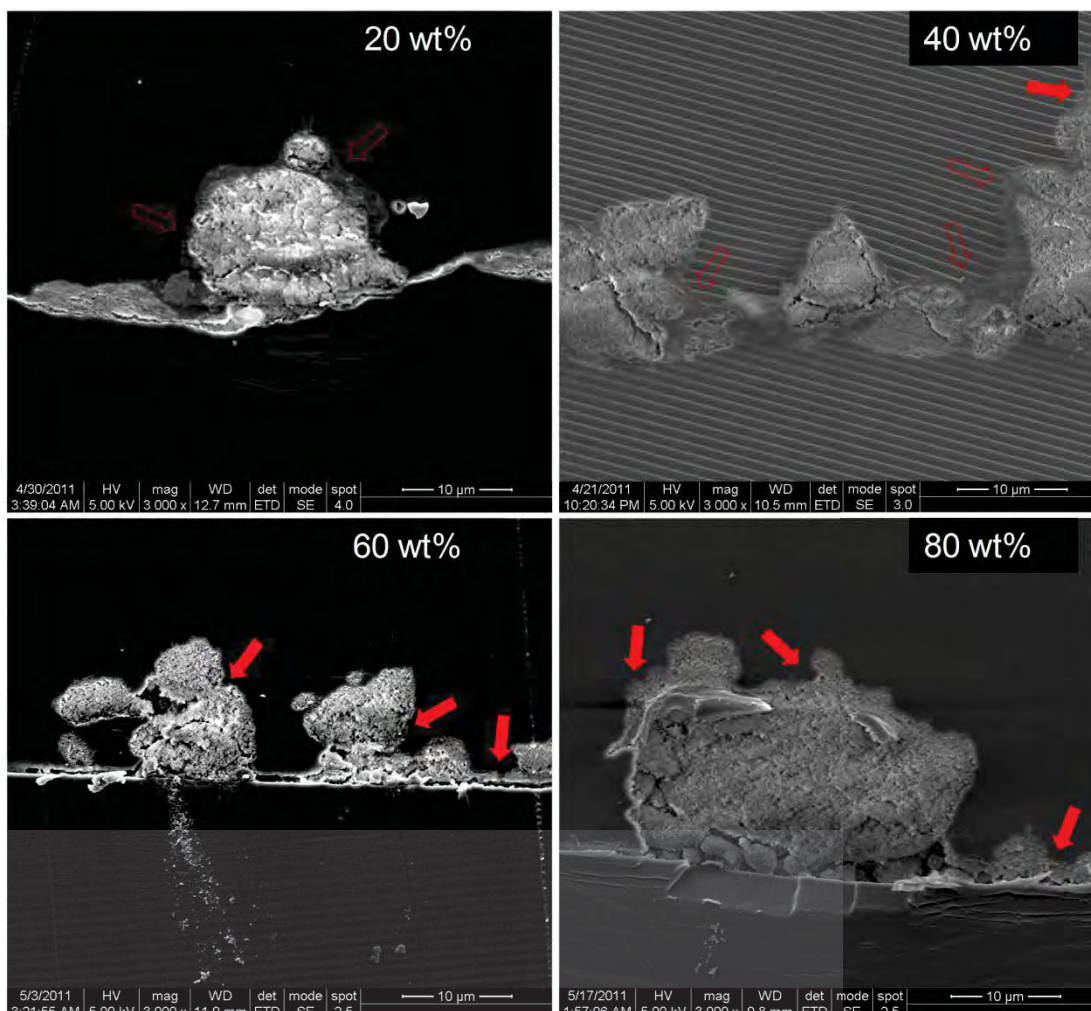


Figure 4. SEM micro-graphs prepared from FF-silica / fluoropolymer coatings mounted in epoxy and cross-sectioned (all at magnification 3000 x). Note the scoring of the epoxy due to the sectioning process, which is helpful in distinguishing it from the fluoropolymer binder that surrounds the silica aggregates. Filled arrows indicate examples of regions where the coating is, if present at all, highly conformal to fine features of the silica surface, whereas unfilled arrows indicate examples where the coating does not conform to the fine features of the silica surface.

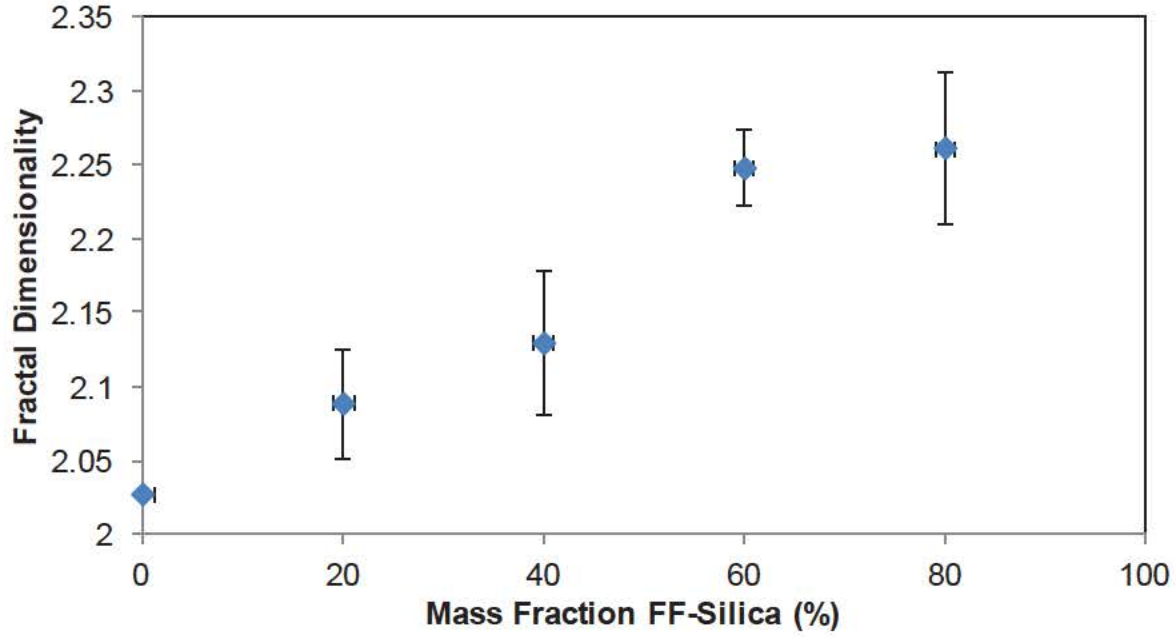


Figure 5. Fractal dimensionality of FF-silica / fluoroelastomer composites as a function of FF-silica loading

Although the exact level of coating conformality is difficult to determine, it is clear from the images in Fig. 4 that even features of $< 1 \mu\text{m}$ are preserved. In accordance with the concept of a minimum wetted pore diameter, which strictly applies only to liquids for which the equilibrium contact angle exceeds 90° , and which should be on the order of $0.1 \mu\text{m}$ for the highly fluorinated aggregates,³³ the surface of any highly conformal coating on the aggregate is also likely to be only partially wet. In terms of the systematic design parameter approach for regularly patterned surfaces, a dimensionless parameter D^* can be defined, based on $\phi_{s,total}$, the fraction of the liquid-solid-air composite interface that is occluded by solid, as

$$D^* = 1 / \phi_{s,total} \quad (1)$$

In most calculations of D^* involving discrete particles on a surface, it is assumed that the surface of each particle is fully wetted, while the spaces between particles remain unwet. However, if the surface is comprised of aggregates, and, due to fine-scale roughness, some fraction “ u ” of the surface of each aggregate remains unwet, then D^* can be expressed in a modified form given by

$$D^* = 1 / [(1-u) \phi_{s0}] = [1 / (1-u)] D_0^* \quad (2)$$

In Eq. (2), the quantities with subscript 0 refer to equivalent values for a surface comprised of monolithic particles with an arrangement identical to that of the aggregates. Because $0 \leq u \leq 1$, D^* will be as high or higher for a surface conformal to aggregates as compared to an identical surface that conforms to monolithic particles. The value of u will depend on specific details of the surface topography at the line of contact,³⁴ not simply the porosity of the aggregate, hence reliable *a priori* methods for calculating u are not readily available. For uniformly distributed, monolithic, and monodisperse spherical particles, however, the parameter D_0^* can be thought of as the square of an effective spacing ratio, that is the distance between particles divided by the particle diameter (see Supporting Information, Section S3). Although these input parameters for D_0^* will not be well-defined for a surface comprised of random, polydisperse (but monolithic) aggregates, the average distance between aggregates will decrease as approximately the square root of the aggregate concentration (for monolayer-like arrangements of aggregates as seen in Fig. 3), while the aggregate size distribution remains constant. The result is that D_0^* should decrease with increased aggregate loading, first rapidly, and then gradually.

By examining Fig. 1 more closely, it can be seen that, once the Cassie state is attained, further increases in silica loading result in modest increases in apparent contact angles. In a composite interface, the higher apparent contact angle results from a decrease in $\phi_{s,total}$, or equivalently, an increase in D^* (see Supporting Information Section S1 and Refs 1-3 for examples). Thus, the experimental data indicate that D^* increases with increased FF-silica loading, contrary to the expected behavior of D_0^* . (A more quantitative approach using equivalent model surfaces is presented in Supporting Information Section S1). Therefore, based on Eq. (1), u must increase with increased FF-silica content. In the specific case of a hierarchical surface with well-defined features replicated at multiple length scales, it has been proven mathematically that u will increase as features are replicated at smaller and smaller length scales.³⁵ The fractal dimensionality of the textured surface also represents another useful single geometric parameter that indicates the level of fine-scale roughness (see Supporting Information Section

S4 for an explanation). Therefore, the increasing fractal dimensionality of the surfaces with increased FF-silica content seen in Fig. 5 implies that u also increases with increasing FF-silica content, and thus explains the observed contact angle behavior. An increasing value of u should also stabilize the Cassie state for lower surface tension liquids, and result in the behavior reflected in Fig. 2.

In addition to the geometric analysis, a careful examination of the cross-sectional images seen in Fig. 4 revealed a qualitative change in the nature of the topography as the FF-silica content was increased. (Note that these changes were seen over the course of examining almost 100 separate images, with Fig. 4 providing representative examples). At loading levels below 40 wt% silica, there appears to be an “excess” of fluoropolymer binder, which fills in small gaps between aggregates and sub-aggregates and provides a relatively thick coating of the substrate that partly submerges the smaller aggregates. The result is a surface that is conformal only above a length scale of a micron or so. Above 40 wt% FF-silica, however, there appears to be almost no “excess” binder. In this case, the highly conformal coating preserves the roughness of the aggregates down to sub-micron scales. Although the most prominent change occurs at approx. 40 wt% FF-silica, where the aggregates also begin to clump together, the coating can be seen to conform to progressively smaller-sized features as the FF-silica loading increases. The gradual spread of conformality to smaller length scales due to an increasingly severe shortage of binder thus appears to be the mechanism responsible for the observed changes in fractal dimensionality, contact angle, and minimum surface tension of contacting fluids exhibiting the Cassie state, as a function of FF-silica loading.

The above discussion illustrates that innovative methods can be utilized to systematically alter the topography of randomly textured surfaces to obtain desired liquid repellence characteristics. Even in the context of spatially-variable robustness, which appears to be characteristic of such surfaces (see the discussion of immersion depth and evaporating droplets in Supporting Information Section S2), it appears that the contact and sliding angles can be altered in systematic fashion by controlling parameters, such as the fractal dimensionality or the distribution of roughness, across multiple length scales. For sprayed on surfaces consisting of rigid aggregates with a polymeric binder, the aggregate to

binder ratio influences these parameters due to a mechanism by which local accumulations of binder mask the fine-scale roughness of the aggregates. The aforementioned mechanism is expected to apply to all types of coatings containing rigid aggregates dispersed in a soft binder, provided that significant migration of binder into large interstices is avoided. Because the mechanism involves a simple excess or shortage of binder, it is expected to be insensitive to the details of the coating process itself, as long as the aggregates are deposited in a monolayer-like fashion.

4. Conclusions

Coatings comprising a sprayed-on mixture of fluoroalkyl-functional precipitated silica and a fluoropolymer binder have proven to be an especially useful class of liquid repellent coating. The combination of low surface energy materials, aggregate porosity, and rapid deposition via spray coating appears to prevent the build-up of binder in interstitial regions, preserving re-entrant curvature across multiple length scales and thereby enabling a wide range of liquid repellency, including superoleophobicity, to be attained via a simple and scalable process. In addition, rather than accumulating in the interstices, the binder becomes widely distributed across the surface of the aggregates, enabling a mechanism in which a simple shortage or excess of binder controls the extent of coating roughness at very small length scales, thereby controlling the extent of liquid repellence. The exploitation of these advantages is expected to lead to significant progress towards large-scale commercialization of superoleophobic surfaces.

Supporting Information Available

Properties of fluoroalkylsilane-functionalized silica (FF-silica, Table S1), complete contact angle data with uncertainties (Table S2), original SEM micrographs of surfaces (Figures S1 and S2), regular geometric model for estimating liquid repellence parameters of FF-silica composites (Section S1), robustness properties of FF-silica composites with accompanying video (Section S2), derivation of the dependence of average distance between particles on particle loading (Section S3), and derivation of the

linkage between fractal dimensionality and extent of fine-scale roughness (Section S4). This material is available free of charge via the Internet at <http://pubs.acs.org>.

Acknowledgements

Support for this work from the Air Force Office of Scientific Research, the Air Force Research Laboratory, Propulsion Directorate, and the National Research Council is gratefully appreciated. The authors thank Mr. Brian Moore of AFRL for helping prepare the video files included in Supporting Information.

References

1. Tuteja, A.; Choi, W.; Ma, M. L.; Mabry, J. M.; Mazzella, S. A.; Rutledge, G. C.; McKinley, G. H.; Cohen, R. E., Designing Superoleophobic Surfaces. *Science* **2007**, *318*, 1618-1622.
2. Tuteja, A.; Choi, W.; Mabry, J. M.; McKinley, G. H.; Cohen, R. E., Robust omniphobic surfaces. *Proc. Nat. Acad. Sci. U. S. A.* **2008**, *105*, 18200-18205.
3. Tuteja, A.; Choi, W.; McKinley, G. H.; Cohen, R. E.; Rubner, M. F., Design Parameters for Superhydrophobicity and Superoleophobicity. *MRS Bull.* **2008**, *33*, 757.
4. Chhatre, S. S.; Choi, W.; Tuteja, A.; Park, K.-C. K.; Mabry, J. M.; McKinley, G. H.; Cohen, R. E., Scale Dependence of Omniphobic Mesh Surfaces. *Langmuir* **2010**, *26*, 4027-4035.
5. Bhushan, B.; Jung, Y. C., Natural and biomimetic artificial surfaces for superhydrophobicity, self-cleaning, low adhesion, and drag reduction. *Prog. Mater. Sci.* **2011**, *56*, 1-108.
6. Zhao, H.; Law, K.-Y.; Sambhy, V., Fabrication, Surface Properties, and Origin of Superoleophobicity for a Model Textured Surface. *Langmuir* **2011**, *27*, 5927-5935.

7. Chhatre, S. S.; Tuteja, A.; Choi, W.; Revaux, A.; Smith, D.; Mabry, J. M.; McKinley, G. H.; Cohen, R. E., Thermal Annealing Treatment to Achieve Switchable and Reversible Oleophobicity on Fabrics. *Langmuir* **2009**, 25 (23), 13625-13632.
8. Choi, B. W.; Tuteja, A.; Chhatre, S.; Mabry, J. M.; Cohen, R.; McKinley, G. H., Fabrics with Tunable Oleophobicity. *Adv. Mater.* **2009**, 21, 2190-2195.
9. Nosonovsky, M.; Bhushan, B., Superhydrophobic surfaces and emerging applications: Non-adhesion, energy, green engineering. *Current Opinion in Colloid & Interface Science* **2009**, 14, 270-280.
10. Howarter, J. A.; Genson, K. L.; Youngblood, J. P., Wetting Behavior of Oleophobic Polymer Coatings Synthesized from Fluorosurfactant-Macromers. *ACS Applied Materials & Interfaces* **2011**, 3, 2022-2030.
11. Tsujii, K.; Yamamoto, T.; Onda, T.; Shibuichi, S., Super oil-repellent surfaces. *Angew. Chem.-Int. Edit. Engl.* **1997**, 36, 1011-1012.
12. Shibuichi, S.; Yamamoto, T.; Onda, T.; Tsujii, K., Super water- and oil-repellent surfaces resulting from fractal structure. *J. Colloid Interface Sci.* **1998**, 208, 287-294.
13. Sheen, Y.-C.; Huang, Y.-C.; Liao, C.-S.; Chou, H.-Y.; Chang, F.-C., New Approach to Fabricate an Extremely Super-amphiphobic Surface Based on Fluorinated Silica Nanoparticles. *J. Polym. Sci. Part B: Polym. Phys.* **2008**, 46, 1984-1990.
14. Steele, A.; Bayer, I.; Loth, E., Inherently Superoleophobic Nanocomposite Coatings by Spray Atomization. *Nano Lett.* **2009**, 1, 501-505.
15. Hsieh, C.-T.; Wu, F.-L.; Chen, W.-Y., Superhydrophobicity and superoleophobicity from hierarchical silica sphere stacking layers. *Mater. Chem. Phys.* **2010**, 121, 14-21.
16. Srinivasan, S.; Chhatre, S. S.; Mabry, J. M.; Cohen, R. E.; McKinley, G. H., Solution spraying of poly(methyl methacrylate) blends to fabricate microtextured, superoleophobic surfaces. *Polymer* **2011**, 52, 3209-3218.

17. Yang, J.; Zhang, Z.; Men, X.; Xu, X.; Zhu, X., A simple approach to fabricate superoleophobic coatings. *New J. Chem.* **2011**, 35, 576-580.
18. Yang, J.; Zhang, Z. Z.; Xu, X. H.; Men, X. H.; Zhu, X. T.; Zhou, X. Y., Superoleophobic textured aluminum surfaces. *New J. Chem.* **2011**, 35, 2422-2426.
19. Deng, X.; Mammen, L.; Butt, H. J.; Vollmer, D., Candle Soot as a Template for a Transparent Robust Superamphiphobic Coating. *Science* **2012**, 33, 67-70.
20. Das, A.; Schutzius, T. M.; Bayer, I. S.; Megaridis, C. M., Superoleophobic and conductive carbon nanofiber/fluoropolymer composite films. *Carbon* **2012**, 50, 1346-1354.
21. Bellanger, H.; Darmanin, T.; Guittard, F., Surface Structuration (Micro and/or Nano) Governed by the Fluorinated Tail Lengths toward Superoleophobic Surfaces. *Langmuir* **2012**, 28, 186-192.
22. Artus, G. R. J.; Zimmermann, J.; Reifler, F. A.; Brewer, S. A.; Seeger, S., A superoleophobic textile repellent towards impacting drops of alkanes. *Appl. Surf. Sci.* **2012**, 258, 3835-3840.
23. Goto, Y.; Takashima, H.; Takishita, K.; Sawada, H., Creation of coating surfaces possessing superhydrophobic and superoleophobic characteristics with fluoroalkyl end-capped vinyltrimethoxysilane oligomeric nanocomposites having biphenylene segments. *J. Colloid Interface Sci.* **2011**, 362, 375-381.
24. Zhu, X. T.; Zhang, Z. Z.; Xu, X. H.; Men, X. H.; Yang, J.; Zhou, X. Y.; Xue, Q. J., Facile fabrication of a superamphiphobic surface on the copper substrate. *J. Colloid Interface Sci.* **2012**, 367, 443-449.
25. Yang, J.; Zhang, Z. Z.; Xu, X. H.; Zhu, X. T.; Men, X. H.; Zhou, X. Y., Superhydrophilic-superoleophobic coatings. *J. Mater. Chem.* **2012**, 22, 2834-2837.
26. Yao, X.; Gao, J.; Song, Y. L.; Jiang, L., Superoleophobic Surfaces with Controllable Oil Adhesion and Their Application in Oil Transportation. *Adv. Funct. Mater.* **2011**, 21, 4270-4276.
27. Yuan, Z. Q.; Xiao, J. Y.; Wang, C. Q.; Zeng, J. C.; Xing, S. L.; Liu, J., Preparation of a superamphiphobic surface on a common cast iron substrate. *J. Coat. Technol. Res.* **2011**, 8, 773-777.

28. Campos, R.; Guenther, A. J.; Haddad, T. S.; Mabry, J. M., Fluoroalkyl-Functionalized Silica Particles: Synthesis, Characterization, and Wetting Characteristics. *Langmuir* **2011**, 27, 10206-10215.
29. See, for example, U. S. Patent 6,025,025 and references therein.
30. Hozumi, A.; McCarthy, T. J., Ultralyophobic Oxidized Aluminum Surfaces Exhibiting Negligible Contact Angle Hysteresis. *Langmuir* **2010**, 26, 2567-2573.
31. Basu, B. B. J.; Paranthaman, A. K., A simple method for the preparation of superhydrophobic PVDF-HMFS hybrid composite coatings. *Appl. Surf. Sci.* **2009**, 255, 4479-4483.
32. The BET surface area of the treated aggregate, as reported in Ref. 25, was 92 m²/g.
33. Smirnov, S.; Vlassiuk, I.; Takmakov, P.; Rios, F., Water Confinement in Hydrophobic Nanopores. Pressure-Induced Wetting and Drying. *ACS Nano* **2010**, 4, 5069-5075.
34. Choi, W.; Tuteja, A.; Mabry, J. M.; Cohen, R. E.; McKinley, G. H., A modified Cassie–Baxter relationship to explain contact angle hysteresis and anisotropy on non-wetting textured surfaces. *J. Colloid Interface Sci.* **2009**, 339, 208-216.
35. Herminghaus, S., Roughness-induced non-wetting, *Europhys. Lett.* **2000**, 52(2), 165.

Supporting Information – Superoleophobic Surfaces through Control of Sprayed-on Stochastic Topography

By Raymond Campos, Andrew J. Guenther,* Adam J. Meuler, Anish Tuteja, Robert E. Cohen, Gareth H. McKinley, Timothy S. Haddad, and Joseph M. Mabry*

Correspondence addresses: andrew.guenther@edwards.af.mil, joseph.mabry@edwards.af.mil

Table S1. Physical and Geometric properties of fluoroalkyl-functionalized silica aggregates used in this work.^{S1}

Silica Type	precipitated (HiSil 233)
Average Diameter (nm)	22
BET Surface Area (m ² /g)	92
BET C Constant	21
Water Vapor Uptake (wt%)	2.8
Wt % Fluorine	9.9
Grafting Density (chains nm ⁻²)	1.6
Graft Layer Molar Volume (cc)	311
Average Thickness of Graft (nm)	0.8

Table S2. Summary of apparent advancing and receding contact angles of water ($\gamma = 72.1$ mN/m), diiodomethane ($\gamma = 50.8$ mN/m), ethylene glycol ($\gamma = 47.7$ mN/m), dimethyl sulfoxide ($\gamma = 44$ mN/m), rapeseed oil ($\gamma = 35.5$ mN/m), hexadecane ($\gamma = 27.5$ mN/m), dodecane ($\gamma = 25.3$ mN/m), and decane ($\gamma = 23.8$ mN/m) on silicon wafers sprayed with FF-silica filled fluoropolymer coatings.

	Water		Diiodomethane		Ethylene Glycol		Dimethyl Sulfoxide	
Sample	θ_{adv}	θ_{rec}	θ_{adv}	θ_{rec}	θ_{adv}	θ_{rec}	θ_{adv}	θ_{rec}
Viton	125 \pm 1	83 \pm 2	102 \pm 1	66 \pm 4	102 \pm 1	56 \pm 6	94 \pm 2	53 \pm 4
10 wt%	141 \pm 2	78 \pm 5	114 \pm 4	52 \pm 5	113 \pm 5	27 \pm 5	108 \pm 3	27 \pm 4
20 wt%	156 \pm 2	151 \pm 3	138 \pm 5	35 \pm 6	147 \pm 3	25 \pm 6	137 \pm 3	13 \pm 5
30 wt%	160 \pm 2	160 \pm 2	146 \pm 4	95 \pm 8	153 \pm 5	139 \pm 8	145 \pm 5	5 \pm 5
40 wt%	159 \pm 1	158 \pm 4	148 \pm 4	133 \pm 6	156 \pm 2	146 \pm 5	156 \pm 2	132 \pm 3
50 wt%	162 \pm 2	162 \pm 3	145 \pm 3	136 \pm 8	154 \pm 4	145 \pm 13	152 \pm 2	133 \pm 9
60 wt%	161 \pm 2	162 \pm 2	152 \pm 2	146 \pm 4	155 \pm 2	145 \pm 7	155 \pm 2	139 \pm 10
70 wt%	168 \pm 3	169 \pm 2	151 \pm 3	148 \pm 4	156 \pm 4	149 \pm 4	157 \pm 1	148 \pm 4
80 wt%	165 \pm 1	165 \pm 1	152 \pm 3	151 \pm 1	157 \pm 2	148 \pm 3	160 \pm 3	153 \pm 6
	Rapeseed Oil		Hexadecane		Dodecane		Decane	
Sample	θ_{adv}	θ_{rec}	θ_{adv}	θ_{rec}	θ_{adv}	θ_{rec}	θ_{adv}	θ_{rec}
Viton	86 \pm 2	42 \pm 3	72 \pm 2	39 \pm 2	70 \pm 3	37 \pm 4	58 \pm 2	24 \pm 3
10 wt%	95 \pm 3	26 \pm 3	82 \pm 3	5 \pm 5				
20 wt%	120 \pm 3	5 \pm 5	101 \pm 3	5 \pm 5				
30 wt%	141 \pm 5	5 \pm 5	126 \pm 3	5 \pm 5				
40 wt%	154 \pm 5	5 \pm 5	135 \pm 4	5 \pm 5				
50 wt%	151 \pm 6	136 \pm 5	144 \pm 4	5 \pm 5				
60 wt%	154 \pm 2	138 \pm 7	155 \pm 1	131 \pm 4	154 \pm 2	89 \pm 16		
70 wt%	156 \pm 2	142 \pm 3	156 \pm 2	131 \pm 5	156 \pm 3	147 \pm 6		
80 wt%	156 \pm 2	153 \pm 2	155 \pm 3	146 \pm 4	162 \pm 2	155 \pm 2	77 \pm 3	5 \pm 5

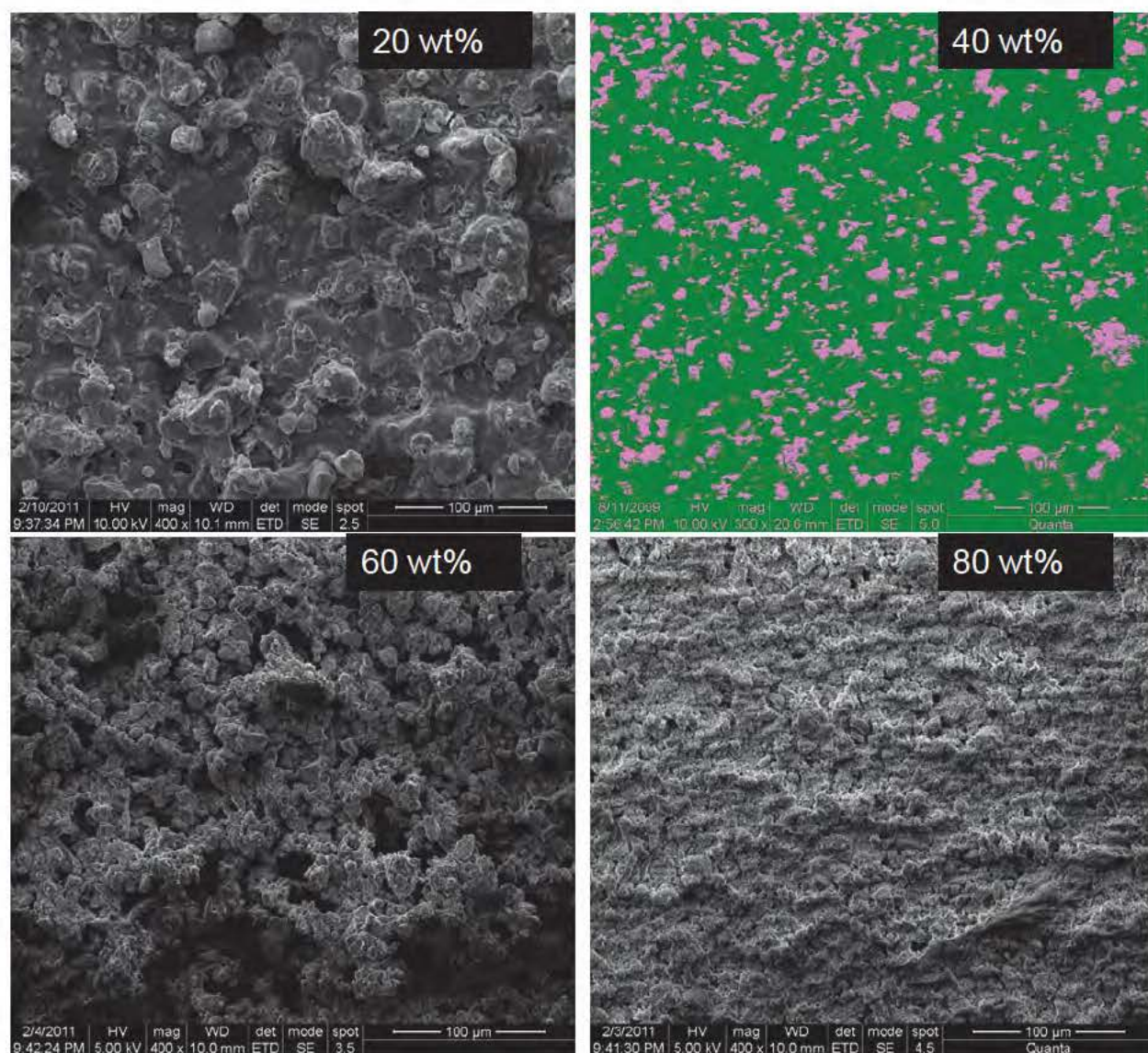


Figure S1. SEM micrographs of FF-silica / fluoropolymer coatings (“top down” view with substrate parallel to the plane of the micrograph). The images in Figure 3 in the main text are cropped and re-sized so as to make for identical magnification and to fit the available space while maximizing viewable details. The flattened and smoothed features at 20 wt% FF-silica are due to the presence of a large excess of binder, which is absent at 40 wt%, 60 wt%, and 80 wt% FF-silica loading levels.

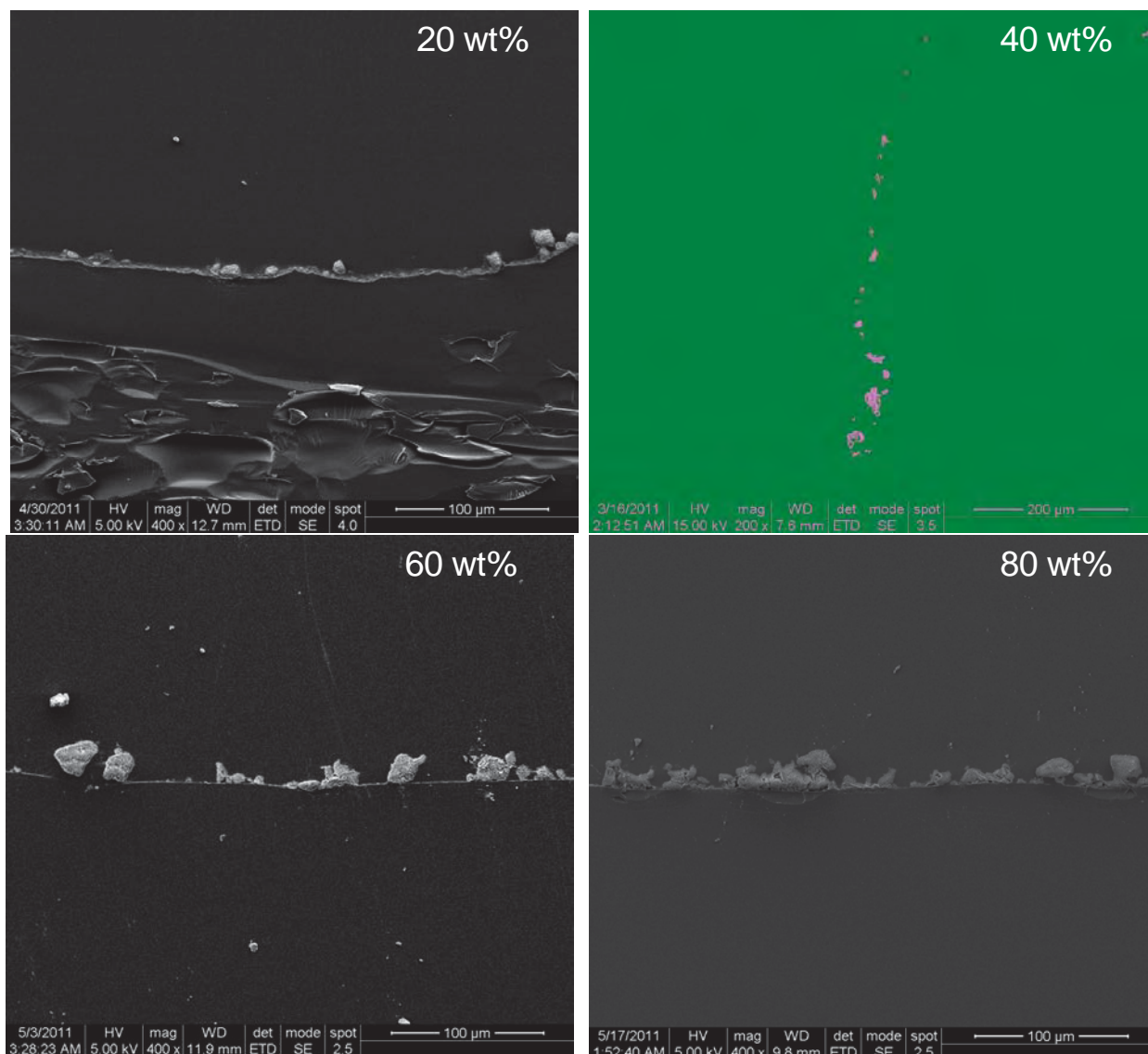


Figure S2. SEM micro-graphs prepared from FF-silica / fluoropolymer coatings mounted in epoxy and cross-sectioned. The images in Figure 3 in the main text are rotated, cropped, and re-sized so as to create identical magnification and orientation, and to fit the available space while maximizing viewable details.

Section S1. Idealized Model to Describe the Wetting Behavior of Spray-Deposited FF-silica Filled Fluoropolymer Coatings

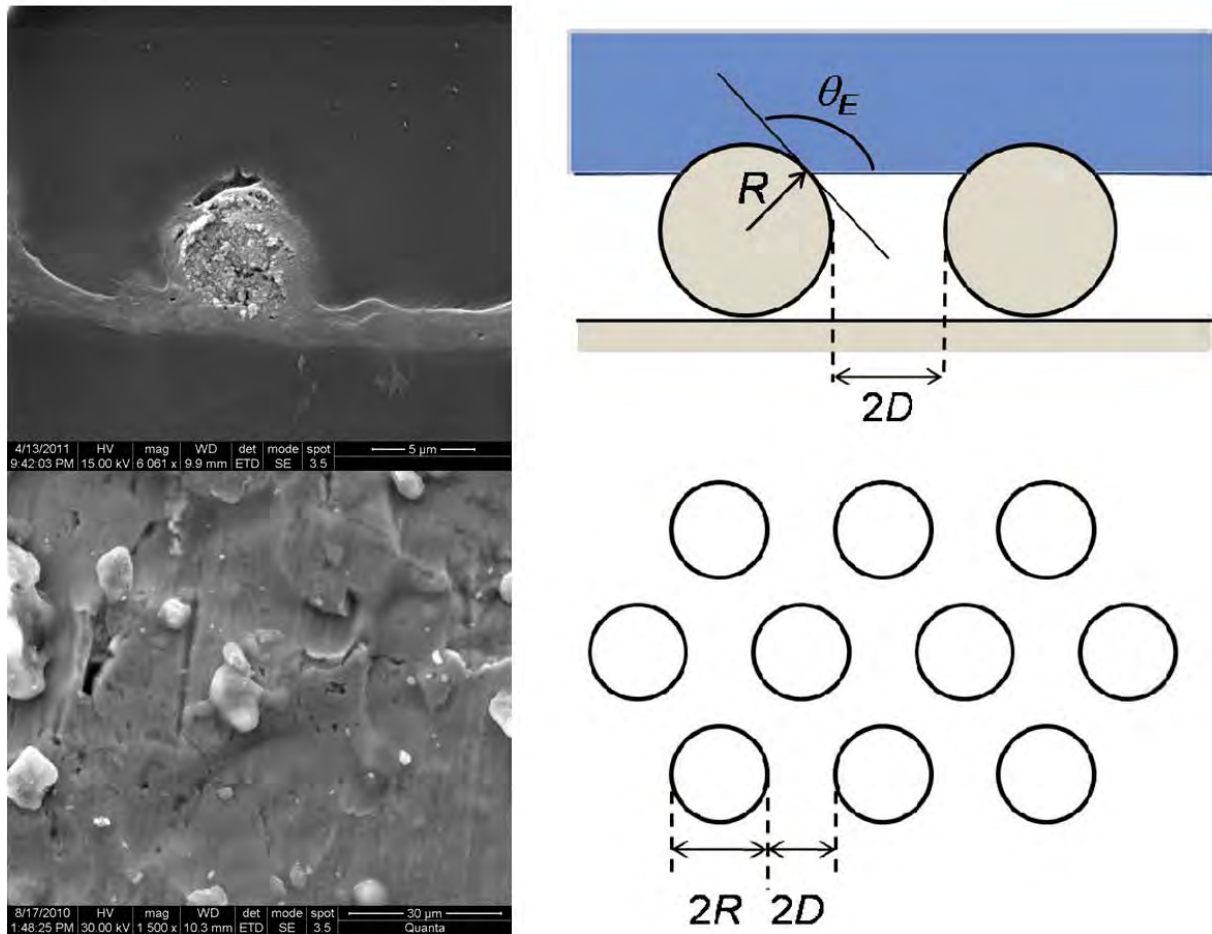


Figure S3. Left: SEM micrographs of spray-deposited FF-silica filled fluoropolymer coatings. Right: Idealized geometric model used to describe the surface of spray-deposited FF-silica filled fluoropolymer coatings.

Spray-deposited coatings of fluoropolymer filled with FF-silica described in the main text demonstrate increased super-liquid repellency with increasing FF-silica content for liquids with decreasing surface tensions, embodied by high apparent contact angles ($>150^\circ$) with low contact

angle hysteresis ($< 10^\circ$) and corresponding low sliding angle. The wetting behavior of these surfaces implies the formation of a composite solid-liquid-air interface between probing droplets and test substrates, with pockets of air being present between micron and sub-micron surface features that possess inherent re-entrant curvature. This system can be described by the Cassie-Baxter relationship in the following form:

$$\cos\theta^* = r_\phi\phi_S \cos\theta_E + \phi_S - 1 \quad (\text{S1})$$

where $\cos\theta_E$ is the contact angle on an identical surface absent of roughness (Young's contact angle), r_ϕ is the roughness of the wetted area, ϕ_S is the area fraction of the liquid-air interface occluded by the solid texture, and $r_\phi\phi_S$ is the fraction of the solid substrate in contact with the liquid.^{S2}

For a model textured surface with a known surface energy, geometric parameters can be included in the Cassie-Baxter equation to accurately predict the apparent contact angle of a millimeter-sized droplet of a given liquid, assuming that θ_E is satisfied locally on micron and sub-micron features.^{S2} Although the coatings described in the present work are devoid of any regularly arranged geometric features, as depicted in the SEM micrographs shown in Figures 3 and 4 of the main text and in Figures S1 through S3, an idealized geometric model may be adopted to elucidate the increased super-liquid repellency as a function of FF-silica content. Features on FF-silica filled fluoropolymer surfaces can be approximately described as a hexagonally-packed array of spheres of diameter $2R$ with a spacing distance of $2D$, as shown in Figure S3. Using this model the Cassie-Baxter equation takes the following form:

$$\cos\theta^* = -1 + 1/D^* [\pi/2\sqrt{3}(1+\cos\theta_E)^2] \quad (\text{S2})$$

where $D^* = [(R+D)/R]^2$, $r_\phi = 2(1+\cos\theta_E)/\sin^2\theta_E$ and $\phi_S = \pi \sin^2\theta_E/2\sqrt{3}D^*$. From this relationship the fraction of liquid in contact with surface is inversely proportional to the spacing ratio, D^* .

The effective spacing ratio of the present on the sprayed surfaces can be calculated by plotting $\cos \theta^*$ vs $[\pi/(2\sqrt{3})](1 + \cos \theta_E)^2$ and fitting a straight line to the data (shown in Figure S4). The slope from the linear fit can then be used to determine the spacing ratio between spherical surface features reported in Table S3.

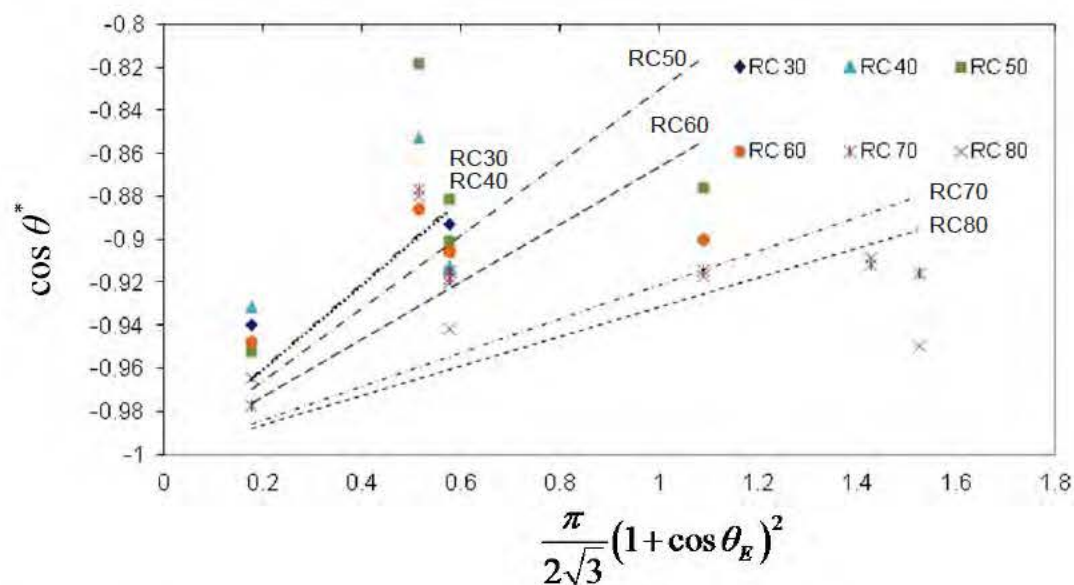


Figure S4. Linear fit used to determine D^* of the idealized surface having the characteristics of the FF-silica / fluoropolymer coatings (herein denoted as “RCxx” where “xx” denoted the weight fraction of FF-silica in the coating).

Table S3. Calculated spacing ratios (D^*) and geometric values (D , R) for spherical features present on sprayed coatings of fluoropolymer filled with various amounts of FF-silica.

Sample	D^*	D (μm)	R (μm)
30 wt%	5 ± 14	360	290
40 wt%	5.1 ± 3.4	320	250
50 wt%	5.9 ± 3.8	250	170
60 wt%	7.5 ± 4.0	210	120
70 wt%	12.7 ± 6.8	100	40
80 wt%	14.6 ± 9.2	90	30

The values in Table S3 are essentially the design parameters for a surface with hexagonally-packed spherical feature with identical surface chemistry as that of the sprayed surfaces reported herein. The spacing ratios for these equivalent surfaces do indeed increase with increasing silica content, consistent with the Cassie-Baxter model. However, these values do not correspond to any obvious features or spacing ratios present in SEM micrographs of the sprayed-surfaces, or to any trends with increasing silica loading. In fact, from top-down and cross-sectional SEM micrographs, the spacing between surface features decreases with increasing FF-silica content, which should increase the wetted fraction when adopting the model presented. However, as mentioned in the main text, the presence of hierarchical roughness, with multiple levels of re-entrant curvature, increases the amount of liquid in contact with micron-sized features which have sub-micron, essentially non-wettable, pores, decreasing the overall wetted fraction with increasing FF-silica loading. The hierarchical nature of these stochastic surfaces prevents a direct comparison to ideal surfaces modeled to-date.

Section S2: Robustness of the Partially Wetted State

The stability of a given composite solid-liquid-air interface can be estimated from a dimensionless “robustness factor” A^* , which is essentially a ratio of the pressure required to distort the liquid-air interface between a probing liquid and test substrate to induce a transition to the Wenzel-state, and the minimum pressure across the interface from the effects of gravity and the Laplace pressure within the droplet; A given droplet is predicted to be in the Wenzel state if $A^* \leq 1$ or in the Cassie-state if $A^* > 1$. From this theoretical framework, one can approximately predict whether a surface with a known, regular surface geometry will be able to support a droplet of a given liquid in the Cassie-state, and what external pressure can be applied before transitioning the droplet to the fully-wetted, Wenzel-state. The pressure required to transition a Cassie-state droplet to the Wenzel-state can be measured with a simple experiment taking advantage of the Laplace pressure present inside of a droplet of liquid ($P_{Laplace} = 2\gamma_{lv}/R_{drop}$). As a droplet of liquid evaporates on a surface, the diameter of the droplet will correspondingly decrease, increasing the pressure imposed on the liquid-air interface. The pressure imposed on the liquid-air interface between the substrate and droplet will increase until the bulging liquid meniscus contacts the unwetted solid substrate below, transitioning the droplet transitioning the droplet to the fully-wetted, Wenzel-state. Such an experiment is illustrated in Figure S5.

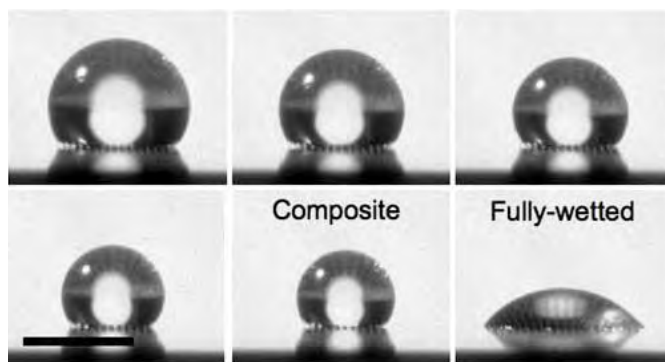


Figure S5. Select still images of a droplet of methanol evaporating on a superoleophobic surface textured with micrometer-sized features possessing re-entrant curvature; At a discrete pressure, the droplet transitions to the fully wetted Wenzel-state (Copyright 2008 National Academy of Sciences, USA).^{S3}

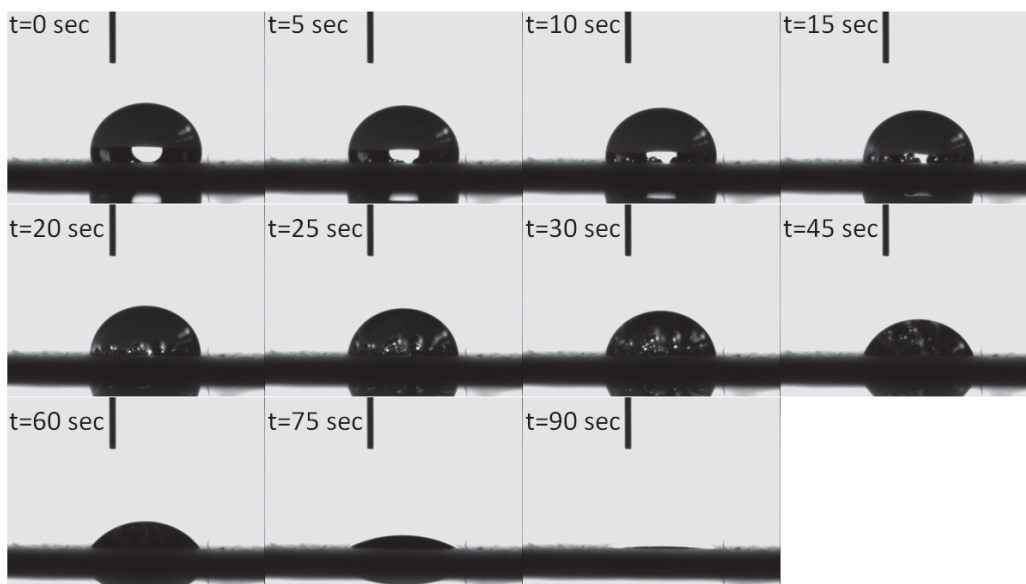


Figure S6. Select images of a chloroform droplet evaporating/infusing into an 80 wt% FF-silica surface displaying the progressive collapse of the metastable solid-liquid-air interface as a result of the increasing Laplace pressure within the droplet. The gradual transition from the Cassie-state to the fully wetted Wenzel-state is accompanied by a continuous reduction of the contact angle and an apparent transfer of air from within surface asperities to inside the droplet. A video has been provided along with the Supporting Information presented herein.

Similar experiments were conducted in an attempt to quantify the super-liquid repellency robustness of the sprayed-coatings reported in this work. However, discrete transitions were not observed for Cassie-state droplets. Instead, a gradual decrease in contact angle was seen for Cassie droplets as a function of decreasing droplet size (increasing Laplace pressure) corresponding to a gradual transition to the wetted state as smaller and smaller levels of hierarchical features are wetted. Representative still images of this experiment can be seen in Figure S7 for a droplet of chloroform evaporating on a spray-deposited surface of fluoropolymer filled with 80 wt% FF-silica. Another interesting observation from Figure S6 is the formation of air bubbles coming out of surface asperities and into the droplet concomitantly with reducing droplet size and contact angle. This observation provides additional evidence that the transition to the Wenzel state does not occur discretely, as with model textured surfaces, but occurs gradually for the sprayed surfaces suggesting that a single breakthrough pressure, or A^* value, cannot be used to describe the surfaces produced in this work. Attempts to measure such breakthrough pressures more directly by slowly immersing samples in increasing depths of fluid also produced variable results, although in some cases stable air pockets remained after immersion in three feet of water.

Additionally, the formation of air bubbles evolving from the occluded surface of the substrate suggests that the pockets of air under the droplet are effectively trapped, unable to escape parallel to the surface when subjected to an external pressure. This observation may help to explain the repellency to low surface tension liquids (such as hexadecane) for which the equilibrium contact angle θ^* is $\ll 90$. Although the surface features present on this surface do not possess ideal geometry for non-wetting surfaces, the liquid-air interface occluded by the

droplet is supported by the increasing pressure of the isolated air pockets as the sagging of the liquid-air interface increases. Therefore, the future design of textured liquid-repellent surfaces may afford increased robustness if low-lying spaces between surface features are isolated from one another, trapping air and preventing the collapse of the composite interface necessary for super-liquid repellency.

Section S3: Simplified Calculation of the Dependence of the Average Distance Between Particles as a Function of Particle Loading in a Stochastic Monolayer

The key assumptions underlying the calculation are as follows:

1. At the largest scale, the surface texture is dominated by protrusions caused by rigid aggregates. Otherwise the surface texture sufficiently far away from the aggregates is relatively flat and smooth as a result of homogeneous film formation of the fluoropolymer binder.
2. Interactions between nearby particles do not create significant new surface texture. Similarly, the surface texture does not depend on the details of the deposition process. Thus, the number of protrusions in the surface is directly proportional to the number density of particles.
3. The overall density of deposited particles is low enough that overlap is rare and can be neglected. In other words, the deposited particles form a sparse monolayer.

The effect of particle loading is computed on the basis of solutions with a constant concentration of solids (c_0) but variable proportion (expressed as a weight fraction w_p) of particles to total solids (particles and binder). Though polydisperse, a sufficient number of

particles exist such that, locally, they are deposited with an average volume (V_p) that changes insignificantly from region to region within the deposited coating. The micrographs shown in Fig. 3 of the main text indicate that the above conditions are satisfied reasonably well for the films under consideration. At higher volume fractions, the tendency of particles to form small, overlapping groups does begin to emerge, but for the present analysis this effect is not considered.

Based on the variables defined above, the average number of particles deposited per unit area of the surface (N_p) is given by:

$$N_p = w_f c_0 V_D / A_D \rho_p V_p \quad (\text{S3})$$

in which V_D and A_D represent the volume of solution deposited and the area over which the deposition occurs, respectively, and in which ρ_p represents the true density of the aggregate, assuming that it is fully wetted by solvent.

If a plane parallel to the substrate is divided on the basis of a well-accepted method such as Voronoi tessellation (that is, into distinct regions defined by the identity of the co-ordinates of the nearest particle center of mass, with one region per particle), then, on the basis of assumptions 1 and 2, there should be exactly one large protrusion per Voronoi polygon on the surface. The distance between protrusions can then be defined on the basis of the characteristic length (d_s) of these polygons, which, given that they are two dimensional, is simply the square root of their mean area (a_s). Since the entire plane is covered by these polygons, the number of polygons per unit area is the same of the number of particles per unit area, and thus the characteristic area of each polygon is simply the inverse of the number per unit area, that is

$$a_s = 1 / N_p \text{ thus } d_s = (1 / N_p)^{1/2} = (A_D \rho_p V_p / w_f c_0 V_D)^{1/2} \quad (\text{S4})$$

For rough surfaces, the geometric parameter D^* used in predicting liquid repellency is typically defined as the ratio of the distance between feature centers (d_s in this case) to the feature size (in one dimension). The characteristic size of each feature will depend on the conformality of the film and the characteristic geometry of the aggregates, but in general should scale with the quantity $V_p^{1/3}$. Hence

$$D^* \sim (A_D \rho_p V_p / w_f c_0 V_D)^{1/2} / V_p^{1/3} \sim (A_D \rho_p / c_0 V_D)^{1/2} V_p^{1/6} w_f^{-1/2} \sim C_I w_f^{-1/2} \quad (\text{S5})$$

where C_I is a constant. Thus, under the assumptions given, D^* will decrease with increasing w_f .

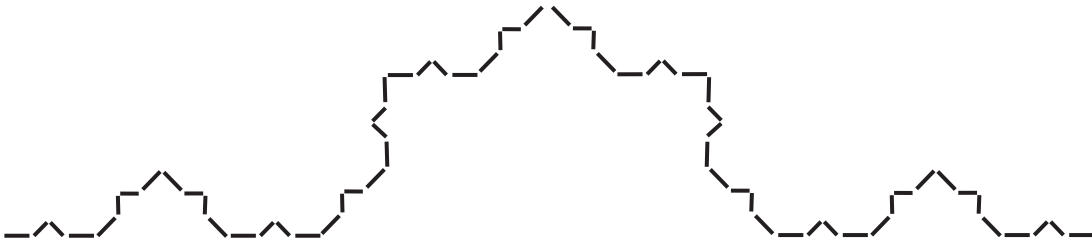
Section S4: Simplified Explanation of the Relationship between Fractal Dimensionality and Fine-Scale Roughness on a Textured Surface

The essence of the box counting routine developed by Shibuichi ^[S4] is that the fractal dimensionality (for a surface formed by iterative convolution of a smaller pattern on to the same pattern repeated at a larger scale) may be defined as $1 + r$, in which r represents the ratio of the cross-sectional path length found by examining the surface on the smaller scale to the path length traced solely by the feature on the larger scale. A simple example is illustrated below.

If a fractal surface is formed by taking the following pattern

For each — substitute — 

which gives rise to a self-similar surface that (up to 3 iterations) appears as:



(Note how the angle of the “steepest” surface features scales with the number of iterations, hence any sufficiently iterated fractal surface should have re-entrance with a minimum re-entrant angle approaching 0°). In the above example, the fractal dimension of the cross-section (using the Pythagorean theorem with an assumed 45° angle between the protruding segments and the background) is $4 / (2 + 2^{1/2}) \approx 4 / 3.4$, since substituting the smaller pattern increases the path length by this ratio. The Shibuichi technique (which, as stated earlier, estimates the fractal dimensionality as $1 + r$) would then yield a fractal dimension of $\approx 1 + 4 / 3.4 \approx 7.4 / 3.4 \approx 2.2$ for this surface (if iterated infinitely).

The Wenzel roughness of the surface (area ratio analogous to r) after only one iteration would also be $\approx 4 / 3.4$, assuming the surface exhibits unidirectional fractal topography (that is, the surface displays a uniform cross-section; for surfaces with multi-directional fractal topography the ratio would be higher but would follow the same trend outlined below). In fact, the Wenzel roughness is given simply by r^n , where n is the number of iterations, in the case of the uniform cross-section. The number of iterations n also defines a convenient scale for the roughness, since each iteration involves shrinking the length scale (in the case above, by a factor of ≈ 3.4). It is clear that, for any value of r modestly greater than one, the function r^n will rapidly increase as n increases, or, as the length scale decreases, with the increases becoming more drastic as the value of r increases. (A similar expression, using the range of length scales rather than number of iterations, is noted by Shibuichi as well as in the earlier work of Onda.^{S5}) Hence, for any surface that may be represented reasonably by an iterated pattern, it is reasonable to conclude that as the fractal dimensionality ($1 + r$) increases, the roughness present at small scales will also increase.

Precipitated silica is an excellent example of an aggregate that can be represented as a fractal system,^{S6,S7} and the surfaces under study are, to a varying degree, conformal with the silica. Moreover, these surfaces do exhibit a characteristic value of r from 1 – 1.3 over a wide range of length scales. Hence, so long as n is reasonably large, an increase in small scale roughness should correlate with increased fractal dimensionality. To estimate n for precipitated silica, the primary particle diameter (22 nm, from Table S1), along with the previously reported^{S6,S7} fractal dimensionality of 1.7-2.4 (estimated here as 2 for simplicity) were used, along with the characteristic aggregate size (10 - 20 μm , see Figure S2). To estimate n , the nature of the iterated structure must also be determined. Since both the primary particles and the primary aggregates tend to be spherical, the repeated unit should be a spherical sub-aggregate. Such sub-aggregates can comprise as few as 4-5 particles or sub-features, but likely not more than 10-20 based on the lack of clearly defined sub-structural levels in precipitated silica aggregates. If N_0 is the number of sub-features that are clustered into the repeated unit, then the total number of particles (N_A) in the complete precipitated silica aggregate is given by $N_A = N_0^n$. In addition, if x_0 represents the diameter of the primary particle and x_A the aggregate diameter, then $N_A = (x_A/x_0)^d$, where d is the fractal dimensionality.

Combining and taking the logarithm yields

$$n \log N_0 = d (\log x_A - \log x_0) \quad (\text{S6})$$

Using base-10 logarithms and the values mentioned previously yields a value of 5-6 for the right hand side of Eq. S6. For $N_0 = 4$, $n \approx 8-10$, while for $N_0 = 20$, $n \approx 4-5$. Hence, a reasonable estimate for n is in the range of 5-10, which is certainly large enough to increase the roughness ratio substantially with increasing fractal dimensionality. For instance, if $r = 1.2$, then the Wenzel roughness r^n will be about 50% greater than if $r = 1.1$ (2.5 vs.1.6) when $n = 5$.

References

- S1. Campos, R.; Guenther, A. J.; Haddad, T. S.; Mabry, J. M., Fluoroalkyl-Functionalized Silica Particles: Synthesis, Characterization, and Wetting Characteristics. *Langmuir* **2011**, *27*, 10206-10215.
- S2. Marmur, A., Wetting on hydrophobic rough surfaces: To be heterogeneous or not to be? *Langmuir* **2003**, *19*, 8343-8348.
- S3. Figure originally published in: Tuteja, A.; Choi, W.; Mabry, J. M.; McKinley, G. H.; Cohen, R. E., Robust omniphobic surfaces. *Proc. Nat. Acad. Sci.* **2008**, *105*, 18200-18205.
- S4. Shibuichi, S.; Yamamoto, T.; Onda, T.; Tsujii, K., Super water- and oil-repellent surfaces resulting from fractal structure. *J. Colloid Interface Sci.* **1998**, *208*, 287-294.
- S5. Onda, T.; Shibuichi, S.; Satoh, N.; Tsujii, K., Super-water-repellent fractal surfaces. *Langmuir* **1996**, *12*, 2125-2127.
- S6. Schneider, G. J.; Fink, S. A.; Rachel, R.; Goritz, D., Three-dimensional structure of precipitated silica as determined by electron tomography. *KGK-Kautsch. Gummi Kunstst.* **2005**, *58*, 461-463.
- S7. Schlomach, J.; Kind, M., Investigations on the semi-batch precipitation of silica. *J. Colloid Interface Sci.* **2004**, *277*, 316-326.